Large forest fires in Canada and the relationship to global sea surface temperatures

W. R. Skinner,[1] A. Shabbar,[1] M. D. Flannigan,[2] and K. Logan[2]

[1] Relationships between variations in peak Canadian forest fire season (JJA) severity and previous winter (DJF) global sea surface temperature (SST) variations are examined for the period 1953 to 1999. Coupled modes of variability between the seasonal severity rating (SSR) index and the previous winter global SSTs are analyzed using singular value decomposition (SVD) analysis. The robustness of the relationship is established by the Monte Carlo technique. The importance of the leading three SVD modes, accounting for approximately 90% of the squared covariance, to Canadian summer forest fire severity is identified. The first mode relates strongly to the global long-term trend, especially evident in the warming of the Southern Hemisphere oceans, and shows significant positive correlation in the forested regions of northwestern, western and central Canada, while southern B.C., the extreme northwest coastal regions of B.C. and Yukon, and the Great Lakes region are identified as having significant negative correlation. The second mode relates to the multidecadal variation of Atlantic SST (AMO) and shows highly significant negative correlation extending from the western NWT and Canadian Prairie Provinces across northern Ontario and Quebec. The third mode is related to Pacific Ocean processes and the interrelationship between El Niño–Southern Oscillation (ENSO) and the Pacific Decadal Oscillation (PDO) and shows strong positive correlation in western Canada and negative correlation in the lower Great Lakes region of southern Ontario and southern Quebec. A 6-month lag relationship between Canadian forest fire variability and large-scale SSTs may provide the basis for developing long-range forecasting schemes for fire severity in Canada.

1. Introduction

[2] Forests cover approximately 45% of the Canadian land area. Wildland fire is a dominant disturbance regime in Canadian forests, particularly in the vast boreal forest region where fire is a process critical to the very existence of primary boreal species such as pine, spruce, and aspen, and is responsible for shaping landscape diversity, and influencing energy flows and biogeochemical cycling [*Stocks et al.*, 2002]. In the early 1990s global biomass burning became recognized as a major perturbation to atmospheric chemistry, with resultant impacts on the earth's physical and chemical climate [*Levine*, 1991, 1996]. It is important to better understand the variability of biomass burning from a global warming perspective.

[3] The number of wildland fires as well as the total area burned by wildland fire in Canada has steadily increased since 1960 with the reported area burned in some regions of the country tripling from 1980 to the present [*Stocks et al.*, 2002]. *Stocks et al.* [1996] examined the spatial distribution of large fires in Canada during the 1980s when an average of almost 10,000 fires burned over 2.8 million hectares annually. They found that by far the greatest area burned occurred in the boreal region of west-central Canada. This was attributed to a combination of factors including fire-prone ecosystems, extreme fire weather, lightning activity, and varying levels of protection in this region. The Canadian fire season is relatively short with the majority of activity from late April through August in the south, and from June to August in the north, when higher temperatures and thunderstorms with lightning strikes occur most frequently [*Stocks et al.*, 2002]. Nearly 50% of the area burned in Canada is the result of fires that are not actioned because of their remote location, low values-at-risk, and efforts to accommodate the natural role of fire in these ecosystems.

[4] A strong relationship between seasonal Canadian temperature and precipitation, key factors in the formation of conditions leading to fire severity, and the ENSO cycle has already been established [*Shabbar and Khandekar*, 1996; *Shabbar et al.*, 1997a]. *Bonsal and Lawford* [1999] have related variations in tropical Pacific SSTs to regional Canadian Prairie dry spells. It is plausible that midlatitude decadal ocean–atmosphere variability could also play an

---

[1]Climate Research Division, Environment Canada, Toronto, Ontario, Canada.
[2]Great Lakes Forestry Centre, Canadian Forest Service, Sault Ste. Marie, Ontario, Canada.
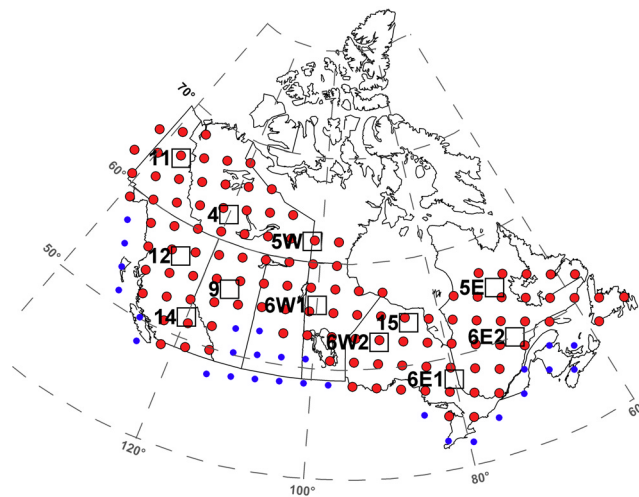
Figure 1. Modified ecozone centroids (squares) used for total area burned (TAB) analysis (refer to Table 1 for ecozone information) and seasonal severity rating (SSR) grid (all dots) at approximately 250 km spacing. Modified ecozones and grid points (large red dots) used in this analysis are based on percent total annual area burned (PAAB) (Table 1). Regions covered by the smaller blue dots were not analyzed also on the basis of PAAB (Table 1).

important role in the establishment and persistence of extended dry spells elsewhere in Canada. Also, sea surface temperature (SST) anomalies in the Pacific have been shown to be associated with atmospheric circulation patterns and thus ridging over western North America in spring and summer [*Bonsal et al.*, 1993]. This affects the weather downstream across much of western and central North America. Recent studies have shown the close geographical association across Canada between anomalous ridging in the midtroposphere at 500 mb and total area burned by wildland fire in the summer season [*Skinner et al.*, 1999, 2002].

[5] *Mestas-Nunez and Enfield* [1999] define the Atlantic multidecadal oscillation (AMO) as the first rotated empirical orthogonal function (EOF) of the global SSTs from which interseasonal ENSO and local trends have been removed. The AMO is a long-timescale oceanic phenomenon with a 65–80 year timescale and 0.48°C range. *Enfield et al.* [2001] have found distinct associations between cold and warm phases of the AMO and the United States summer rainfall and river flows. This Atlantic atmosphere-ocean long-term variability may also provide additional information about summer moisture patterns and forest fire severity in Canada. *Shabbar and Skinner* [2004] have examined the relationship between Canadian drought patterns (Palmer Drought Severity Index) and global SST anomalies for the period 1940–2001 and have found one Atlantic and two Pacific SST modes responsible for moisture availability in three key regions of Canada: extreme northwestern Boreal, western Boreal, and the Great Lakes–St. Lawrence region.

[6] The purpose of this study is to compare the total area burned (TAB) statistic, as taken from the Canadian Large Fire Database (LFDB) [*Stocks et al.*, 2002], and the seasonal severity rating (SSR) [*Van Wagner*, 1987] index as calculated from meteorological observations and then to use

the SSR index to determine the spatial patterns and temporal variability of summer (June–August) fire severity in Canada from 1953 to 1999. Singular value decomposition (SVD) of the joint structure between Canadian summer (JJA) fire severity data and global winter (DJF) SSTs is used to quantify the impact of ENSO and midlatitude ocean-atmosphere variability on seasonal forest fire severity in Canada. Additionally, structures in fire severity related to global warming, as manifested by long-term changes in global SSTs, are also examined. It is hoped that the coupled patterns obtained by identifying the source of global SST variability in the preceding winter months (December–February) will provide useful insights toward developing a seasonal and possibly a multiyear fire severity prediction scheme in Canada, as well as a useful tool to managers for warm season planning. The utility of the prediction is enhanced since there is a 6-month lead between the SST predictor and the SSR, giving ample time for planning activities. The remainder of the paper is organized as follows: the data sets and SVD methodology are described in section 2, the results are highlighted in section 3, and a discussion and summary in section 4.

2. Data and Methods

2.1. Canadian Forest Fire Data

[7] Two measures of forest fire severity were used in this study. The first, total area burned (TAB) by wildland fire was tabulated monthly and seasonally by ecozone and modified ecozone (Figure 1). The distribution of these data is poor for advanced statistical analysis (low number of points and irregular spatial distribution). As a result, a second measure of forest fire severity was employed, the seasonal severity rating (SSR) index, which has a much larger number of points and more comprehensive spatial distribution (Figure 1). These two measures of forest fire severity are fully described in the following subsections and are compared statistically in section 3.2.

2.1.1. Large Fire Database (LFDB)

[8] The Canadian Large Fire Database (LFDB) is a record of reported fires in Canada that exceed 200 ha in size [*Stocks et al.*, 2002]. Because the record lengths vary by reporting provincial agency, analysis of TAB data is restricted to 1959 to 1999, the common period of complete national data coverage in the database from all reporting agencies. TAB was the initial forest fire variable in this analysis. It is a function of many factors, some of which are not dependent on the weather. Area burned across a landscape is determined by a complex set of variables including the weather, the size of the sample area, the period under consideration, the extent of the forest, the topography, fragmentation of the landscape (rivers, lakes, roads, agricultural land), fuel characteristics, season, latitude, fire suppression policies and priorities, fire control, organizational size and efficiency, fire site accessibility, ignitions (people and lightning), and simultaneous fires.

[9] Pertinent information in the LFDB includes precise spatial coordinates, start date of the fire, total area burned, the cause of the fire if known, and the ecozone and ecoregion in which the majority of the fire burned. Recent studies have examined the TAB from the LFDB in relation to classified patterns of 500 mb circulation [*Skinner et al.*,

Table 1. Percent Annual Area Burned (PAAB) by Ecozone and Modified Ecozone From *Stocks et al.* [2002]

Ecozone	Ecozone Number	Area Burned, ha	Percent Total, %	Cumulative Percent Total, %
Boreal Shield West	6W	17,717,927.78	26.85	26.85
Taiga Plains	4	14,953,149.43	22.66	49.52
Taiga Shield West	5W	10,476,899.39	15.88	65.40
Boreal Plains	9	7,339,506.41	11.12	76.52
Taiga Shield East	5E	4,374,786.52	6.63	83.15
Boreal Cordillera	12	4,178,129.41	6.33	89.48
Boreal Shield East	6E	3,772,168.35	5.72	95.20
Hudson Plains	15	1,591,178.99	2.41	97.61
Taiga Cordillera	11	958,437.96	1.45	99.06
Montane Cordillera	14	498,416.31	0.76	99.82
Southern Arctic	3	37,249.85	0.06	99.87
Atlantic Maritime	7	36,793.99	0.06	99.93
Pacific Maritime	13	33,496.60	0.05	99.98
Prairies	10	11,855.78	0.02	100.00
Mixedwood Plains	8	445.16	0.00	100.00

2002], for the projection of future area burned in Canada from global climate models (GCM) [*Flannigan et al.*, 2005], and to demonstrate the effects of human-induced climate change on Canadian forest fires [*Gillett et al.*, 2004]. For this study, lightning caused fires were analyzed at the ecozone level, and in some cases the subecozone level (Figure 1). The ecozone configuration was used in this study because this classification is based largely on vegetational distribution.

[10] TAB was tabulated for monthly periods for May to September by ecozone [*Ecological Stratification Working Group*, 1996] and modified ecozone. Ecozones where total cumulative May-August area burned composed 99.82% of the national total were used in this study (Figure 1 and Table 1). This closely coincides with those ecozones where the percent annual area burned (PAAB) is greater than approximately 1.0% of the national total [*Stocks et al.*, 2002]. Ecozone 5, the Taiga Shield, was modified by dividing it into east and west components separated by Hudson Bay. Ecozone 6, the Boreal Shield, was also modified by dividing it into two eastern and two western components, at 95°W, 87°W (near Lake Nipigon), and 75°W as there are significant differences in fire activity, and climate, between eastern, central and western regions of this ecozone [*Harrington et al.*, 1983]. The Montane Cordillera in southern B.C. (ecozone 14) was analyzed in this study as it represented close to 1% PAAB (Table 1). Monthly area burned totals were then totaled for the peak fire season (June–August). This period best represents major fire activity across the entire country. The natural logarithm of the area burned (ha) was used to normalize area burned because the raw area burned distribution is bimodal.

2.1.2. Seasonal Severity Rating (SSR)

[11] The severity of a fire season is a function of a number of factors including the weather, ignition (patterns and types), fuel characteristics (fuel type, structure and moisture) and human activities such as fire management. The weather is the key factor in determining the severity of the fire season [*Flannigan and Wotton*, 2001].

[12] The Daily Severity Rating (DSR) was developed to provide a measure of the difficulty in suppressing a forest fire [*Williams*, 1959; *Van Wagner*, 1987] and is calculated from the Fire Weather Index. The 1200 LST observations of temperature, relative humidity, wind speed, and 24-hour precipitation are the inputs required to calculate the com-

ponents of the Canadian Forest Fire Weather Index (FWI) System [*Van Wagner*, 1987]. The FWI System is a weather-based system that models fuel moisture using a dynamic bookkeeping system that tracks the drying and wetting of distinct fuel layers in the forest floor. There are three moisture codes that represent the moisture content of fine fuels (Fine Fuel Moisture Content, FFMC), loosely compacted organic material (Duff Moisture Code, DMC) and a deep layer of compact organic material (Drought Code, DC). The drying time lags for these three fuel layers are 2/3 of a day, 15 days and 52 days, respectively. These moisture indexes are combined to create a generalized index of the availability of fuel for consumption (Build Up Index, BUI) and the FFMC is combined with wind to estimate the potential spread rate of a fire (Initial Spread Index, ISI). The BUI and ISI are combined to create the FWI which is an estimate of the potential intensity of a spreading fire. The Daily Severity Rating (DSR) is a simple exponential function of the FWI intended to increase the weight of higher values of FWI in order to compensate for the exponential increase in area burned with fire diameter [*Williams*, 1959; *Van Wagner*, 1970]. Because the DSR is most sensitive to variations in air temperature and relative humidity [*Flannigan and Van Wagner*, 1991] it is considered a useful index for examining SST relationships. These two elements are the leading characteristics of air mass and can vary greatly from region to region depending on antecedent global SST configurations.

[13] The DSR has been calculated from Environment Canada synoptic weather data from 1953 to 1999 and interpolated to a grid using a thin-plate cubic-spline method [*Flannigan and Wotton*, 1989]. This method was found to be the best suited interpolation technique applied to a multivariate index of this type. A minimum of 12 weather stations were used for each grid point interpolation though more were used if available. The weather stations closest to the grid point were chosen first using an expanding search radius until at least 12 active stations were found. The interpolated data were then averaged monthly and seasonally to yield the Seasonal Severity Rating (SSR). The SSR can be used as an objective measure of the fire weather/climate from season to season and region to region. Figure 1 shows data gridded across Canada on an approximate 250 km spacing used in this study. Grid points designated with large red dots were used in this study. Regions covered

by the smaller blue dots were not used as the PAAB is less than 1.0% (Table 1) [*Stocks et al.*, 2002].

[14] The SSR can also be useful for historical analysis and in long-range forecasts for use as a management tool. High SSR values often correspond to greater fire severity and vice versa. Correlations found in this study based on the relatively short 47-year SSR time series could be misleading, especially when establishing relationships with longer-period multidecadal modes such as AMO. However, on a preliminary basis, and on the shorter term, the associations are considered useful.

2.2. Global SST Data

[15] Extended reconstructed global sea surface temperature [*Smith and Reynolds*, 2003] anomalies are analyzed for the 1940–2002 period, where the anomalies are calculated relative to the 1960–1990 base period. For the 1940–1997 period, in situ observations from a new version of COADS release 2 [*Woodruff et al.*, 1998] are used together with an eigenvector reconstruction [*Smith et al.*, 1998]. The reconstruction of the data involves a rigorous quality control procedure and a statistical analysis methodology which is an improvement over their previous version [*Smith et al.*, 1996]. Data from 1998 to 2002 are based on in situ observations and satellite estimates, which are combined using the optimum interpolation method as described by *Reynolds et al.* [2002]. The joined SST data are then analyzed at 2° resolution. *Smith and Reynolds* [2003] show that the resulting SSTs are capable of resolving dominant modes of climate variability.

2.3. Methods

[16] Large-scale relationships between winter (DJF) patterns of global SSTs and following summer (JJA) fire patterns in Canada are analyzed for the 41-year period 1959 to 1999 for TAB data, and for the 47 year period 1953 to 1999 for SSR data by SVD analysis (also known as Multiple Correlation Analysis in the literature [*von Storch and Zwiers*, 1999]). The SVD analysis is used to identify and compare the modes of variability in the fire and SST anomaly data. A similar technique has been used by *Wallace et al.* [1992] and *Iwasaka and Wallace* [1995] to identify large-scale relationships between SST and 500 hPa height anomalies and heat flux and atmospheric circulation, respectively. A mathematical description of SVD analysis can be found in the Appendix of *Iwasaka and Wallace* [1995].

[17] The SVD method aims to relate two fields by decomposing their covariance matrix into singular values and two sets of paired orthogonal vectors, one for each field. The covariance between the expansion coefficients of the leading pattern in each field is maximized. The singular values give the magnitude of the squared covariance fraction (SCF) as accounted for by the various singular values [*Bretherton et al.*, 1992; *Wallace et al.*, 1992]. The square of any singular value between two fields for a given mode is indicative of the fraction of the total squared covariance accounted for by that mode. The teleconnections between the two fields are discerned by the spatial patterns of the heterogeneous correlation, which is defined as the serial correlation between the expansion coefficients of one field and the grid point anomaly values of the other field

$r[\text{FIRE}_k(t), \text{SST}_i(t)]$ and $r[\text{SST}_k(t), \text{FIRE}_i(t)]$, where k and i refer to mode and grid number respectively.

[18] The heterogeneous correlation patterns for the *n*th mode in the SVD expansion indicate how well the pattern of anomalies in the FIRE (SST) field can be specified on the basis of the *n*th expansion coefficient of the SST (FIRE) field. In the spatial domain, the loading maps for a given field are mutually orthogonal. Heterogeneous correlation patterns for the first three modes in the direct SVD expansion are analyzed for statistical evidence of teleconnections between the two fields. The homogeneous correlation pattern indicates the spatial pattern of the variations associated with the time series of the mode in the same field. The structure of both heterogeneous and homogeneous correlation patterns tends to be the same if the correlation between the amplitude time series of the given mode is high and significant. In this study, we will focus on the heterogeneous correlation patterns between the summer fire data (TAB and SSR) and global SST anomalies.

3. Results

3.1. SVD Analysis of Canadian TAB and SSR Fire Data and Global SST Data

[19] Two separate SVD analyses were performed to identify large-scale relationships between the fire and SST data sets. The first examined the TAB data, while the second examined the SSR data, both with the same global SST anomaly data set. Prior to the SVD analysis, the dimensionality of fire and SST data sets was reduced by the EOF analysis. The first 10 EOF modes of the summer fire (TAB and SSR) and winter SST were chosen as input into the SVD procedure. In the first analysis, the first 10 EOF modes of summer fire total area burned (TAB) accounted for 98.3% of the TAB variance while the first 10 EOF modes of winter SST accounted for 71.4% of the SST variance. In the second analysis, the first 10 EOF modes of summer fire seasonal severity rating (SSR) accounted for 82.7% of the TAB variance while the first 10 EOF modes of winter SST accounted for 70.0% of the SST variance. Most of the variance, however, is concentrated in the first three EOFs, with 57.0% of the total variability for summer TAB and 44.7% of the total variability for winter SST in the first SVD analysis and 51.5% of the total variability for summer SSR and 44.4% of the total variability for winter SST in the second SVD analysis.

[20] The SVD analysis is used to identify and compare the coupled modes of variability in the fire severity and SST anomaly data. SVD methodology always gives a mathematical solution, and it is recognized that there is a chance that the resulting pair of coupled patterns may be nothing more than a mathematical artifact [*Cherry*, 1997; *Newman and Sardeshmukh*, 1995]. The geophysical interpretation of the coupled patterns, however, can be aided by comparison of the results from the EOF analysis, where the time expansion of summer fire severity EOFs are correlated with the winter anomaly field of the SSTs and vice versa.

3.2. Comparison of TAB and SSR

[21] The time series of summer TAB from 1959 to 1999 and summer SSR from 1953 to 1999 for Western Canada (west of 87°W), are compared in Figure 2. Western Canada
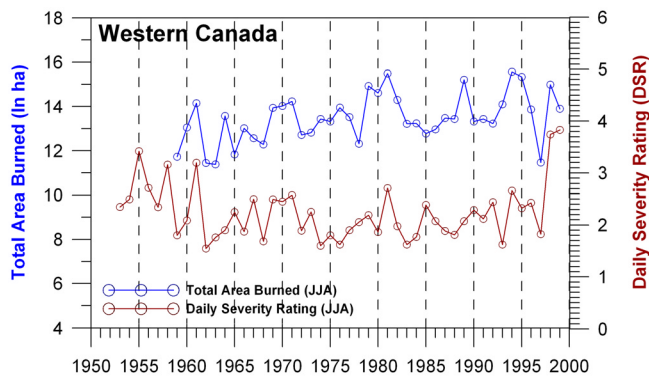
Figure 2. Summer (JJA) total area burned (TAB) from 1959 and seasonal severity rating (SSR) from 1953 for western Canada west of 87°W.

is analyzed because greater than 90% of the percent annual area burned (PAAB) is accounted for by the ecozones west of Lake Nipigon [*Stocks et al.*, 2002] (see also Table 1). The TAB and SSR series have a modest correlation (r = +0.47) for the overlapping period 1959–1999. Both TAB and DSR have generally increased since the late 1950s, although the extreme high values in 1998 and 1999 give the impression of even greater increase in SSR over time. There is an indication from the DSR curve of higher fire severity during the 1950s prior to the TAB record.

[22] Assessment of the similarity between the two measures of forest fire severity can also be made by comparing the results from the SVD analysis of TAB and global SST anomalies with SSR. The time expansion of the first three modes of summer TAB are correlated with the time series of SSR anomalies at each grid point. Figures 3a–3c show the correlation fields between the TAB time series for the first three patterns (SVP1, SVP2, and SVP3), respectively, and individual grid point for each SSR pattern for the overlapping 41 year period 1959–1999. Strong correlations are evident and the resulting spatial patterns closely resemble the SVD patterns of SSR for 47 summer seasons 1953 to 1999 (Figures 4a–4c in the next section) and reinforce the usefulness of the SSR index as a suitable modeled proxy for the observed TAB. In addition, the global SST spatial patterns (not shown) of the two SVD analyses closely resemble one another. There are strong associations between SVP1(TAB) and SVP2(SSR), SVP2(TAB) and SVP3(SSR), and SVP3(TAB) and SVP1(SSR). This is also confirmed by time series correlation (also not shown).

3.3. SVD Results

[23] The SVD analysis of TAB at the ecozone and modified ecozone level and global SST anomalies was performed but is not shown as the summary statistics closely resemble those for the SVD analysis of gridded SSR data and global SST anomalies. Figure 4a shows that the spatial pattern associated with *S*1(SSR), explaining 11.1% of the total variance of Canadian SSR, has a north-south dipole across most of Canada with positive loadings over much of the forested regions of the country and negative loadings over most of southern Canada. Opposite negative loadings are especially evident in southern B.C. and extreme southern Ontario and Quebec. The time series

for *S*1(SSR) shows evidence of strong positive trend. It will be shown that this mode of the SSR has its origin mainly in the global-scale long-term trend.

[24] Figure 4b shows the spatial pattern associated with *S*2(SSR) (16.5% of the total variance) identifies mainly negative loadings across Canada with stronger negative loadings in northwestern Canada (northern Saskatche-
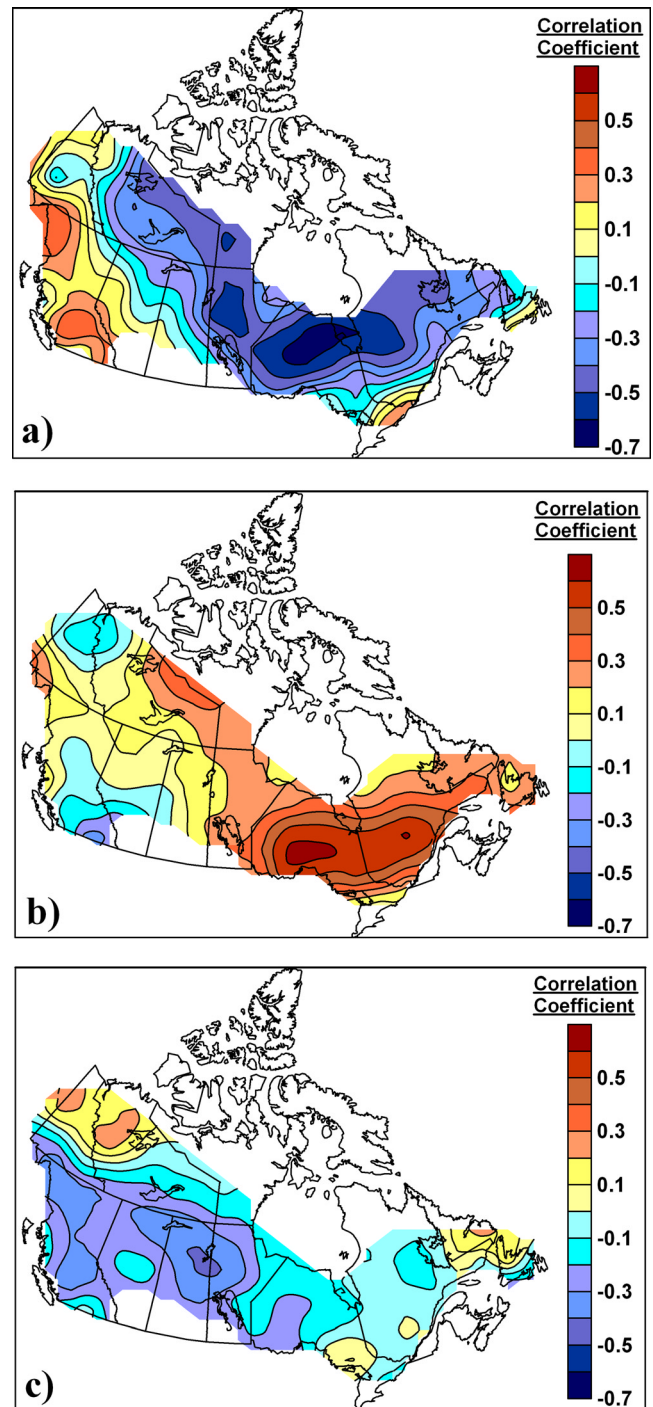

Figure 3. (a) Correlation field between SVP1 total area burned (TAB) time series and grid point seasonal severity rating (SSR) for 47 year period 1959–1999, (b) same as Figure 3a but for SVP2 (TAB), and (c) same as Figure 3a but for SVP3. The contour interval is r = 0.1.

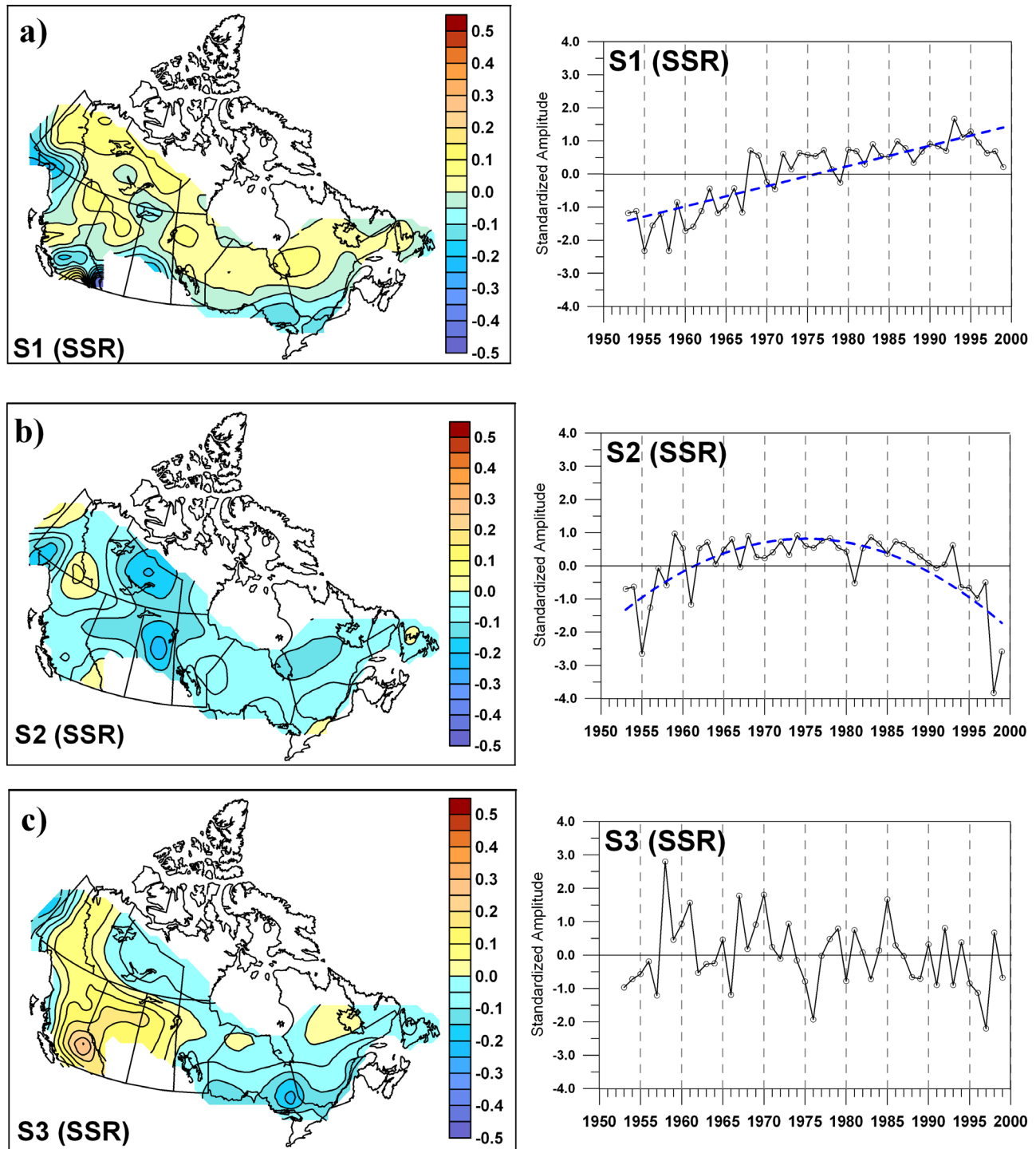**Figure 4.** (a) First SVD pattern (S_1) of SSR and standardized amplitude based on data for 47 summer (JJA) seasons 1953–1999, (b) same as Figure 4a but for the second SVD pattern (S_2) of SSR and standardized amplitude, and (c) same as Figure 4a but for the third SVD pattern (S_3) of SSR and standardized amplitude. The contour interval is 0.05.

wan–NWT) with a reversal to slight positive loadings in the extreme northwest. The time series for $S2$(SSR) shows evidence of multidecadal variability with extreme conditions in 1955 and 1998–1999. It will be shown that this mode of the SSR has its origin mainly in Atlantic Ocean processes, namely the Atlantic Multidecadal Oscillation (AMO) phenomenon.

[25] Figure 4c shows that the spatial pattern associated with $S3$(SSR) (11.5% of the total variance) identifies an east-west gradient with opposing loadings in eastern Canada (negative) and western and northwestern Canada (positive). The time series for $S3$(SSR) shows little evidence of trend but considerable interannual variability. It will be shown that this mode of the SSR has its origin in the Pacific Ocean
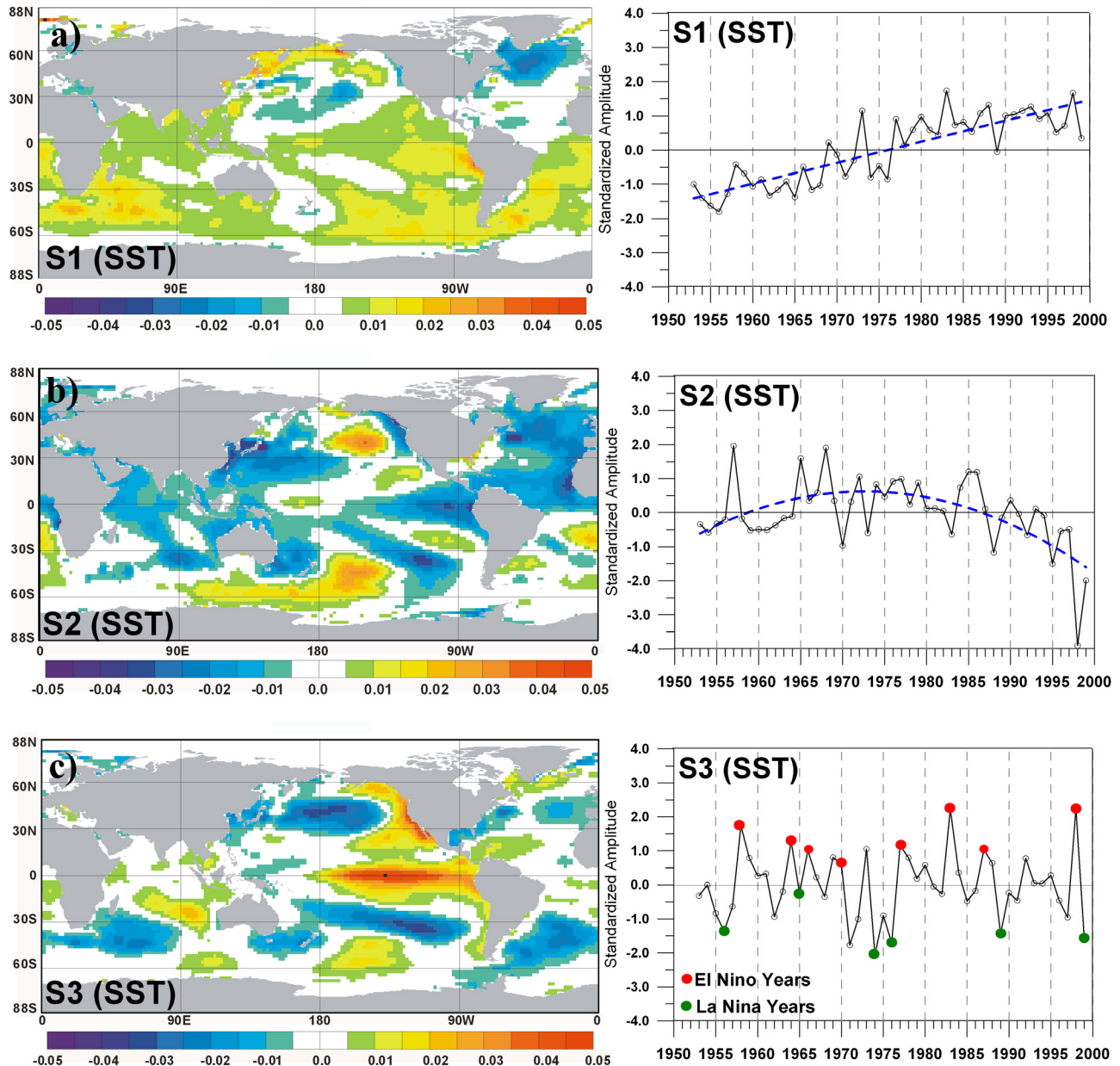
Figure 5. (a) First SVD pattern (S_1) of SST and standardized amplitude based on data for 47 winter (DJF) seasons 1953–1999, (b) same as Figure 5a but for the second SVD pattern (S_2) of SST and standardized amplitude, and (c) same as Figure 5a but for the third SVD pattern (S_3) of SST and standardized amplitude. The contour interval is 0.05.

processes, mainly the Pacific Decadal Oscillation (PDO) and El Niño–Southern Oscillation (ENSO) phenomena.

[26] The spatial pattern, or trend at every grid point, associated with $S1$(SST), explaining 15.1% of the total variance of global winter SST variability, is shown in Figure 5a. It identifies distinct trends in the SSTs with strong positive loadings throughout the Southern Hemisphere oceans, and negative loadings in the north Atlantic and north-central Pacific Oceans. A similar SST loading pattern has been reported by *Smith and Reynolds* [2003]. They identified a trend mode in their second rotated EOF of the global SSTs. The time series for S1(SST) exhibits strong positive trend.

[27] Figure 5b exhibits the spatial pattern associated with $S2$(SST) (7.2% of the total variance). The dominant feature is the AMO pattern with strong negative loadings in the entire north Atlantic relative to the scattered distribution of negative loadings across the remainder of the global oceans. There may be other physical processes inherent in this mode that are likely reflected by covariability in the western Pacific. However, the main source of variability is in the Atlantic where there is a pattern reminiscent of the AMO signal. The time series shows evidence of multidecadal variation with decreasing values over the past two decades. The change in the time coefficient is likely associated with the variability of the Atlantic processes at varying time-

scales as previously identified by *Shabbar and Skinner* [2004]. The role of the atmosphere in the north Atlantic sector in determining the underlying oceanic variability on an interannual timescale has also been shown in a number of studies [e.g., *Czaja and Marshall*, 2001; *Hurrell*, 1996]. While examining variability of the 500-hPa geopotential heights in the western Atlantic, *Shabbar et al.* [1997b] found a similar change in their Baffin−west Atlantic circulation index in the early 1970s.

[28] The spatial pattern associated with $S3$(SST) (17.4% of the total variance) is shown in Figure 5c. It identifies strong positive loadings in the tropical Pacific Ocean from 180°W to the coast of South America (warm ENSO) and along the North America west coast, with another opposing negative center in the north Pacific (positive PDO). Previous studies have identified the coexistence of these two sources of variability. *Zhang et al.* [1997] found a similar mode while examining wintertime variability in the high-pass (interannual) filtered SSTs. Pacific SST variations dominate this mode, including the effects of ENSO in the eastern equatorial Pacific and the extratropical SST fluctuations in the central north Pacific, resembling the coupled ocean−atmosphere mode known as the Pacific decadal oscillation (PDO) [*Mantua et al.*, 1997]. This mode also includes a component of the interannual variability as reflected by a broader and weaker center in the eastern tropical Pacific. The tropical loadings in $S3$ are located entirely east of the International Date Line. *Deser and Blackmon* [1995] identify this pattern in the Pacific basin SSTs as their second EOF. This pattern also bears a striking resemblance to the low-pass (interdecadal) filtered SSTs in the Pacific basin as identified by *Zhang et al.* [1997]. *Deser and Blackmon* [1995] also report an interannual ENSO pattern as their leading mode of Pacific basin SSTs. The time series associated with this mode also identifies extremes in ENSO years. Warm El Niño (positive) and cold La Niña (negative) ENSO events are also identified.

[29] Table 2 provides the three main summary statistics of the SVD analysis for SSR. These statistics provide a measure of the strength of the relationship between the two fields. The first statistic, the squared covariance fraction (SCF$_k$), where k is the mode number, provides the percentage of the total squared covariance between the two fields explained by the SVD mode, and is proportional to the square of its singular value. This is a measure of the relative importance of the SVD mode in the relationship between the two fields. It is clear from Table 2 that the squared covariance is concentrated in the first three modes (close to 90%). Thereafter, the squared covariance statistic drops off sharply thus signifying the importance of the first three modes in determining SSR variability. The second statistic is the correlation coefficient (r_k) between the two time series that represent the temporal variations of the mode in the two fields. It is a measure of the similarity between the time variations of the patterns of the two fields, or how strongly the two fields are related to each other. The values remain near 0.5 (significant at the 5% level) for the first four modes. The third statistic, the normalized root-mean-squared covariance (NCF$_k$), is the ratio of the squared singular value of the mode to the greatest possible total squared covariance of the matrix. It is a measure of the absolute importance of the SVD mode in the relationship

Table 2. Summary Statistics of SVD Analysis for Canadian Gridded Seasonal Severity Rating (SSR) Data and Global SST Anomaly Data, 1953–1999

Mode (k)	Squared Covariance Fraction SCF, %	Correlation Coefficient	Normalized Squared Covariance Fraction NCF, %
1	48.78	0.77	9.93
2	25.29	0.66	7.15
3	15.14	0.39	5.53
4	4.40	0.47	2.98
5	2.75	0.38	2.36

between the two fields and is the most revealing statistic in the analysis. Approximately 23% of NCF is concentrated in the first three modes of the SVD expansion. The values are about equally distributed and drop off in higher modes, again emphasizing the importance of these modes in relation to higher modes. While examining relationships between surface heat flux over the north Pacific and 500-hPa geopotential heights and SSTs, *Iwasaka and Wallace* [1995] found that the significant NCFs were in the range of 8%−14%.

[30] The robustness of these results is established by the Monte Carlo technique, as suggested by *Barnett and Preisendorfer* [1987]. Test results on 1000 Monte Carlo SVD expansions, in which the time coefficient of the SSR series is randomly shuffled, show that the r_k and NCF$_k$ statistics in all three modes of the SSR and global SST anomaly data are statistically significant at the 5% level, with the exception of mode 3, which is not significant even at the 10% level. The p values are, for mode 1 = 0.03, mode 2 = 0.006, and mode 3 = 0.247. The (NCF$_k$) 5% confidence level for $NCF_1 = 9.47$, $NCF_2 = 5.77$, and $NCF_3 = 4.26$ (see Table 2 for comparison). The SCF$_k$ statistics for the first and second modes are also significant at the 5% level. Two further tests are performed in section 3.5 in order to validate the teleconnection patterns found in the SVD analysis.

3.4. Teleconnection Between Canadian Fire Severity and Global SST Patterns

[31] The heterogeneous correlation patterns show how the two fields are related to one another and how much of the amplitude of the variations is explained by the SVD mode. Figures 6a−6c show the heterogeneous correlation patterns for each of the first three modes in the SVD expansion for winter global SST anomaly data and for the following summer SSR data from 1953 to 1999. Each map represents the correlation between the expansion coefficients of one field and the grid point anomaly values of the other field.

[32] The heterogeneous pattern for the first SVD mode (Figure 6a) has two prominent features, the warming of the Southern Hemisphere oceans, as indicated by the positive loadings, mainly south of the equator, and the negative loadings in the north Atlantic and north-central Pacific. Statistics calculated in Table 2 mark this mode as the most important singular mode in the relationship between the two fields accounting for almost 50% of the squared covariance and correlation coefficient r = 0.78. Positive SSR correlation (high fire severity corresponding to strong warming trend, and vice versa) is identified throughout the forested regions of northwestern, western and central Canada. Negative SSR correlation (low fire severity corresponding to strong warm-
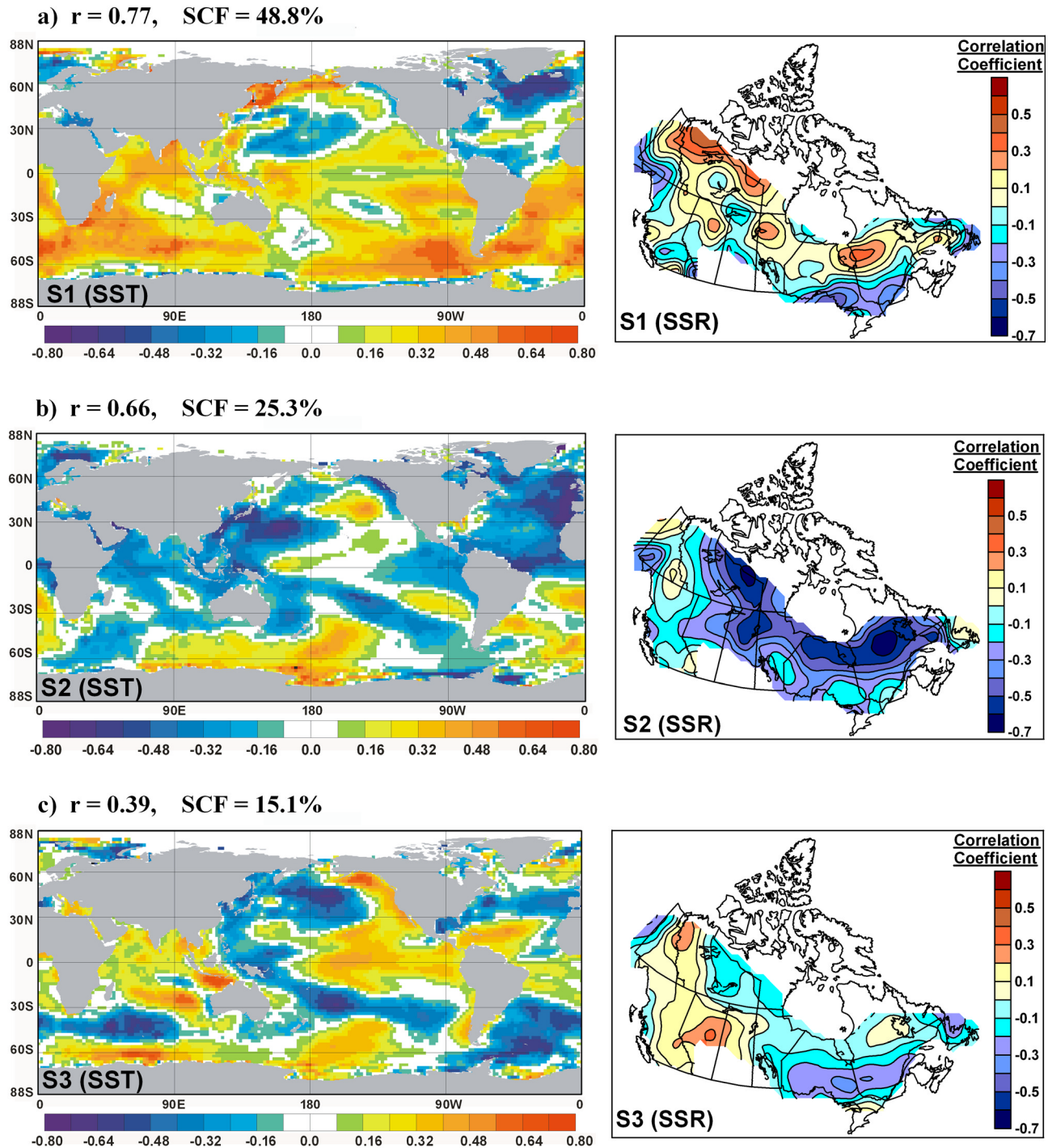
Figure 6. (a) Heterogeneous correlation pattern for the first mode in the direct SVD expansion using global SSTs. The temporal correlation coefficient between the corresponding expansion coefficients $r(SSRk\ SSTk)$, where k refers to the mode number, and the SCF (%) are shown. (b) Same as Figure 6a but for the second mode and (c) same as Figure 6a but for the third mode. The contour interval for the SST maps is r = 0.08 and the contour interval for the SSR maps is r = 0.1.

ing trend, and vice versa) is evident in southern B.C., the extreme northwest coastal regions of B.C. and Yukon, and in the Great Lakes−St. Lawrence region.

[33] The heterogeneous correlation pattern for the second SVD mode (Figure 6b) has strong negative loadings over the entire north Atlantic and is indicative of cooling.

Shabbar and Skinner [2004] have related the north Atlantic feature to the influences of the AMO. The accompanying SSR pattern shows quite strong negative correlations (high fire severity corresponding to strong cooling trend, and vice versa) in an area stretching from the western NWT and Canadian Prairie Provinces across northern Ontario and
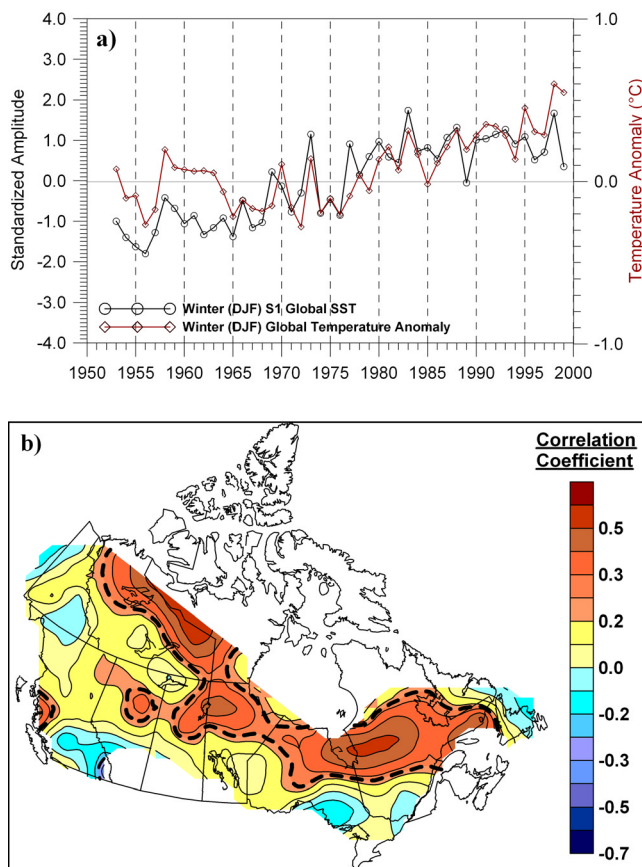
Figure 7. (a) Winter season (DJF) globally averaged temperature anomalies relative to the 1961–1990 mean and the time coefficient of winter S1 SST pattern and (b) correlation pattern between winter globally averaged temperature anomalies and the following summer SSR. Regions of Canada with significant correlations at the 5% level are indicated by dashed lines. The contour interval is r = 0.1.

Quebec. While examining the summer precipitation during the second half of the twentieth century, *Zhang et al.* [1997] also found a tendency toward drying throughout the same region. In the following section, it will be shown that the centers over west-central Canada and over the lower Great Lakes and the St. Lawrence valley are more closely related to the variability in the AMO.

[34] The heterogeneous pattern for the third SVD mode (Figure 6c) identifies ENSO variability in the tropical Pacific and interdecadal variability in the central north Pacific. This mode shows that the positive phase of the PDO, along with the warm phase of ENSO, as identified by *Zhang et al.* [1997] and *Deser and Blackmon* [1995]. It leads to a high SSR over southwestern, western, and northwestern Canada, and lower SSR over south-central and southeastern Canada (Ontario and Quebec).

3.5. Validation of Results

[35] The SVD method clearly identifies the main features of SST variability when examining SSTs on the global scale. The first and most dominant mode, explaining approximately 49% of the squared covariance, is related

mainly to the strong trend primarily in the Southern Hemisphere oceans. Mainly Atlantic processes (AMO) are identified in the second mode, explaining approximately 25% of the squared covariance, while the influences of ENSO and the interdecadal PDO dominate in the third mode, explaining approximately 15% of the squared covariance. Two tests were performed to validate that the large-scale processes obtained here are not mere artifacts of the SVD analysis.

[36] The first validation test was to examine more closely regional-scale (entire Atlantic and north Pacific) SST variability (not shown). In the analysis of the entire Atlantic basin SSTs with SSR, the first two SVD modes explained over 80% of the squared covariance and compared closely to modes S1 (trend) and S2 (AMO), respectively, as identified in the global SST analysis. Correlation of S1 global with S1 Atlantic is r = 0.88, while correlation of S2 global with S2 Atlantic is r = 0.85, both significant at better than the 5% level. In the analysis of north Pacific SSTs (north of 20°N), the first two modes explained greater than 75% of the squared covariance and compared closely to modes S1 (trend) and S3 (PDO and ENSO) in the global analysis. Correlation of S1 global with S1 north Pacific is r = 0.89, while correlation of S3 global with S2 north Pacific is r = 0. 57. Both are significant at better than the 5% level. It should be noted that the likely reason for the lower correlation between the S3 global and S2 north Pacific is the tropical Pacific is not included in the regional analysis thus filtering the ENSO influence. In addition, the corresponding heterogeneous correlation patterns with SSR were closely similar to those realized from the global SST analysis.

[37] The second validation test was to examine the relationships between indices of common large-scale forcing mechanisms and the SST and SSR time series and patterns identified in the SVD analysis. In this study, the first and most dominant mode (S1) is related mainly to the global SST trend with strong positive loadings in the Southern Hemisphere oceans and negative loadings in the north Atlantic and north-central Pacific. Figure 7 provides evidence concerning the influence of the global trend inherent in the S1 patterns (Figures 4a and 5a). Plotted on Figure 7a are the time series of winter season globally averaged temperature anomalies relative to the 1961–1990 mean [*Folland et al.*, 2001] and the time coefficient of winter S1 SST pattern. The globally averaged temperature curve is closely associated with S1(SST) (r = +0.71) and is significant at the 5% level. Figure 7b shows the correlation pattern between the winter globally averaged temperature anomalies and following summer SSR at each Canadian grid location. Regions of Canada possessing statistically significant values at the 5% level are outlined by dashed lines. The effect of the global trend is seen most clearly in the boreal and taiga regions of northern Quebec and Ontario, the Hudson Bay Lowlands, northern Manitoba and Saskatchewan and northern NWT. The correlation pattern across Canada is quite similar to that found in the heterogeneous correlation SSR pattern for the first mode in the direct SVD expansion SSTs (Figure 6a).

[38] The second mode (S2) in this study relates mainly to Atlantic processes (AMO). Figure 8 provides evidence concerning the AMO structure inherent in the S2 patterns (Figures 4b and 5b). Plotted on Figure 8a are the winter
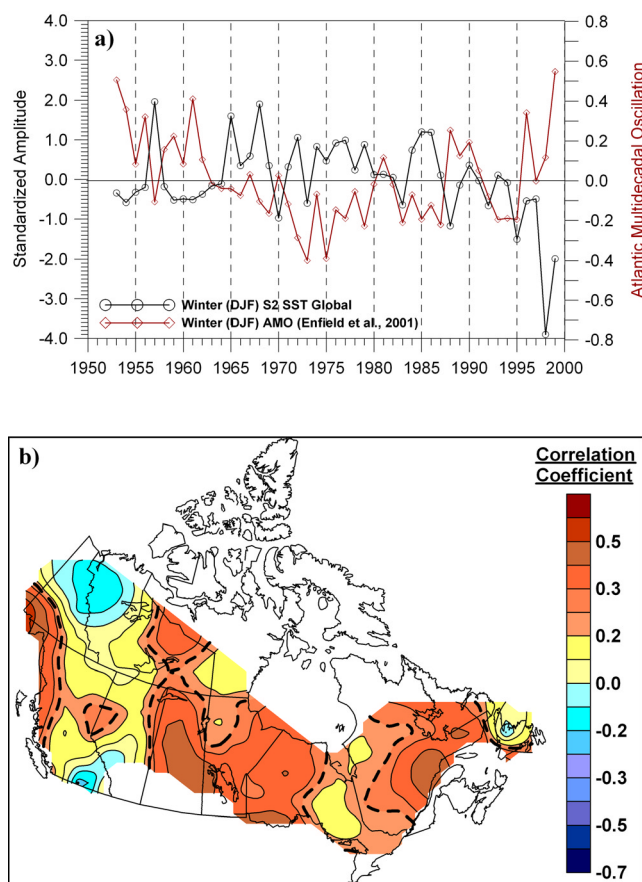
Figure 8. (a) Winter season (DJF) AMO and the time coefficient of winter S2 SST pattern and (b) correlation pattern between winter AMO and the following summer SSR. Regions of Canada with significant correlations at the 5% level are indicated by dashed lines. The contour interval is r = 0.1.

AMO index [*Enfield et al.*, 2001] and the time coefficient of winter S2 SST pattern. The two time series track each other fairly well with a moderate correlation of r = −0.43, significant at the 5% level. The AMO warm phase from the 1950s to early 1960s is associated with lower SSR conditions, while the cool phase from the 1960s to the 1990s is related higher SSR conditions (see Figure 2). Finally, the return to a warm AMO phase in the late 1990s is linked with lower SSR conditions. *Enfield et al.* [2001] also found a negative correlation between the AMO time series and the Climate Division rainfall over the northeastern United States.

[39] Figure 8b shows the correlation pattern between the winter AMO index and following summer SSR at each Canadian grid location. Regions of Canada possessing statistically significant values at the 5% level are outlined by dashed lines. The effect of AMO is seen most clearly with the most robust impact evident over the boreal forest region of Saskatchewan, Manitoba and northwestern Ontario, as well as the lower St. Lawrence valley of Quebec and extending into southern Labrador. Significant negative correlation seen in extreme NW Canada possibly reflects the positively correlated co-oscillation in north Pacific with the AMO, as suggested by *Enfield et al.* [2001]. This spatial

signature is very similar to that found by *Shabbar and Skinner* [2004] for Canadian drought (PDSI) and AMO. Also, the correlation pattern in Figure 8b is similar to that found in the heterogeneous correlation SSR pattern for the second mode in the direct SVD expansion SSTs (Figure 6b) as well as the second SVD pattern (S2) of SSR (Figure 4b). The physical mechanisms responsible for varying climatic conditions in regions located considerably downstream from the Atlantic, in a generally west-to-east atmospheric circulation, are not clearly understood and require further research.

[40] The influences of ENSO and the interdecadal PDO dominate the third mode (S3). Figure 9 provides evidence concerning the ENSO and PDO structures inherent in the S3 patterns (Figures 4c and 5c). Plotted on Figure 9a is the winter ENSO index (Climate Diagnostics Center http://www.cdc.noaa.gov/ClimateIndices/) and the time coefficient of winter S3 SST pattern. The Nino1+2 extreme eastern tropical Pacific SST index was used because it provided the best correlations with both the time coefficient of winter S3 SST pattern and following summer SSR. In addition, the location of Nino1+2 corresponds with that of the ENSO signal identified in Figure 5c. Several indices of winter (DJF) ENSO were analyzed (i.e., Nino3+4, SOI, MEI) and the strongest and most spatially extensive signal was found with Nino1+2, although similar spatial patterns of summer SSR were found with all other indices.

[41] Plotted on Figure 9b is the winter PDO index [*Mantua et al.*, 1997] and the time coefficient of winter S3 SST pattern. The close association between S3 and ENSO is clearly evident (r = +0.91). The correlation between S3 and PDO is more moderate (r = +0.58). Both correlations are significant at the 5% level. The interannual ENSO, the decadal PDO, and the interrelationship between the two play a significant role in the determination of the summer moisture availability in Canada [*Shabbar et al.*, 1997a; *Shabbar and Skinner*, 2004]. Warm ENSO (El Niño) events lead to a summer moisture deficit in the western two thirds of Canada and northern Ontario and Quebec. Conversely, cold ENSO (La Niña) events produce an abundance of summer moisture, mainly in extreme western Canada and in the southeastern portions of the Canadian Prairies.

[42] Figure 9c shows the correlation pattern between the winter ENSO index and following summer SSR, at each Canadian grid location, while Figure 9d shows the correlation pattern between the winter PDO index and following summer SSR, at each Canadian grid location. Regions of Canada possessing statistically significant values at the 5% level are outlined by dashed lines. The effect of the Pacific processes is seen most clearly with positive correlations in western Canada (Alberta, Saskatchewan and northwestern NWT and northern Ontario and Quebec), and negative correlations in the lower Great Lakes region of southern Ontario and central Quebec, with the most robust impact evident over the northern Prairie provinces and western NWT and northern Quebec (Figure 9c). Previous studies [*Shabbar and Khandekar*, 1996; *Shabbar et al.*, 1997a] have identified the ENSO effect on air temperature and precipitation in Canada to be strongest in the southern prairie provinces, a region that is blanked in this study (Figure 1) because of low PAAB (Table 1). The correlation patterns are both quite similar to those found in the
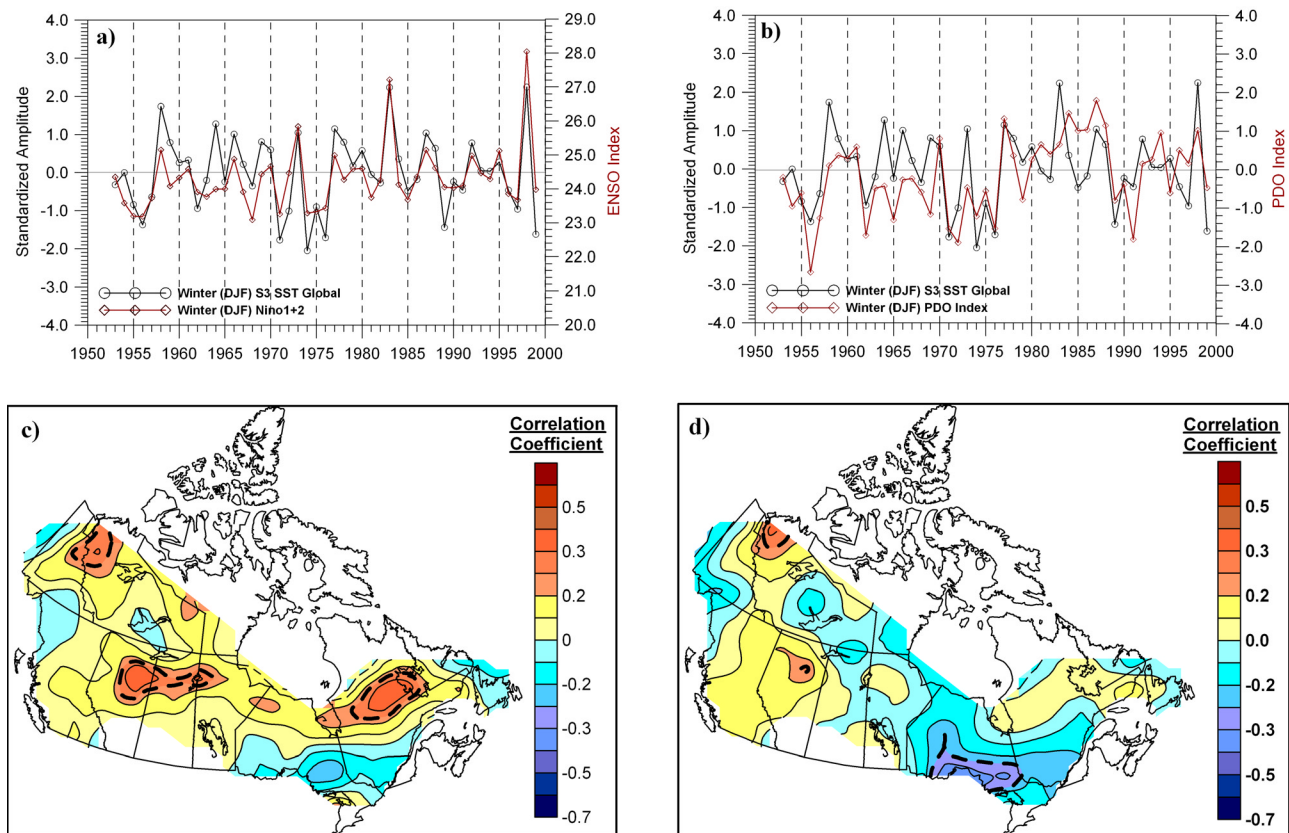
Figure 9. (a) Winter season (DJF) ENSO and the time coefficient of winter S3 SST pattern, (b) same as Figure 9a but for winter season (DJF) PDO, (c) correlation pattern between winter ENSO and the following summer SSR, and (d) correlation pattern between winter PDO and the following summer SSR. Regions of Canada with significant correlations at the 5% level are indicated by dashed lines. The contour interval is r = 0.1.

heterogeneous correlation SSR pattern for the third mode in the direct SVD expansion (Figure 6c).

4. Discussion and Summary

[43] This study has determined the spatial patterns of summer forest fire severity in Canada as represented by the seasonal severity rating (SSR). The SSR is essentially a multivariate meteorological index combining the elements of air temperature, humidity, rainfall, and wind speed, over both short (hourly/daily) and long timescales (weekly/monthly/seasonal), that influence the moisture content of potential fire fuels. This SSR index compares quite favorably with actual observed measurements of TAB and appears well suited for historical analysis and potential predictability on a seasonal scale. In addition, this study has identified the source of variability in global SSTs in the preceding winter months. Large-scale relationships between summer SSR patterns in Canada and previous winter global SST patterns are then analyzed using SVD analysis. The resulting coupled patterns provide insight into the teleconnection patterns between Canadian forest fire severity and global SSTs. It is found that the long-term trend in the global oceans, especially present in the Southern Hemisphere, Atlantic multidecadal variability (AMO), and the interannual and interdecadal variability in the Pacific basin

(ENSO and PDO) play prominent roles in affecting summer fire severity conditions.

[44] Recently, *Hoerling and Kumar* [2003] have linked the droughts that occurred from 1998 to 2002 in certain areas of the midlatitudes to common global oceanic influences. In particular, observation and modeling results relate the cold ENSO-like conditions to drought in the southwestern United States, Europe and southwest Asia. The leading three SVD modes of Canadian summer forest fire severity and global SST explain almost 90% of the squared covariance between the two fields. The first field is related to the SST trend in the global southern oceans and accounts for approximately one half of the squared covariance. Previous studies [*Skinner et al.*, 1999, 2002; *Podur et al.*, 2002; *Stocks et al.*, 2002; *Gillett et al.*, 2004] have demonstrated the upward trend in area burned (TAB) by wildland fires in Canada over the past three decades. This study has found favorable statistical association between the SSR index and the TAB record (Figures 2–4) and has used it in this analysis as a modeled proxy indicator of observed historical forest fire severity for Canada. In a recent study, *Gillett et al.* [2004] demonstrated that human-induced climate change has significantly affected the area burned by forest fires in Canada by first using output from a coupled climate model to show that greenhouse gas and sulfate aerosol emissions have made a detectable contribution to summer season

warming in regions of Canada where the area burned by forest fires has increased and then applying a statistical model to simulate temperature changes.

[45] The second field is related mainly to Atlantic processes and accounts for approximately one quarter of the squared covariance. A long-timescale oceanic phenomenon referred to as the AMO, the first rotated EOF of Atlantic SSTs, has been found with a 65–80 year timescale and a range of 0.4°C [*Enfield et al.*, 2001]. The signal is most intense in the North Atlantic, but is global in scope, with a positively correlated co-oscillation in the North Pacific. Figure 8b reveals strongly correlated regions in eastern and central Canada summer SSR with the winter AMO index. *Shabbar and Skinner* [2004] identified very similar regions to be associated with AMO in the study of Canadian drought, especially in eastern Canada.

[46] The third field is related to Pacific Ocean processes and the interrelationship between ENSO and the PDO and explains approximately 15% of the squared covariance. The lagged relationship between winter ENSO/PDO and summer Canadian SSR is at least partially supported by the connection between the tropical and the north Pacific through the atmospheric bridge concept of *Lau and Nath* [1994]. The results of this study show that the warm phase of ENSO and positive phase of PDO leads to dry conditions and higher fire severity in western and northwestern Canada as well as northeastern Canada. Conversely, the cold phase of ENSO and negative PDO produces an excess in summer moisture and low fire severity over western Canada and the southeastern areas of the Prairie Provinces.

[47] In order to gain confidence in the mathematical solution given by the SVD methodology, the geophysical relevancy of the coupled patterns should also be investigated [*Cherry*, 1997]. It is recognized that the coupled modes found in this study are subject to the constraint of the number of EOFs chosen for the SSTs and SSR fields as input into the SVD technique, as well as the mathematical constraint of the SVD itself. Two tests were performed to validate that the large-scale processes obtained here are not mere artifacts of the SVD analysis, a regional SST analysis and examination of the relationship between indices of common large-scale forcing mechanisms and the SST and SSR time series and patterns identified in the SVD analysis. The recovery of the dominant features shown in Figures 4–6 lends credibility to the dynamical significance of the coupled modes. One of the aims of this study was to lay the groundwork for the development of long-range fire severity prediction in Canada. The SVD technique is easy to apply for finding coupled patterns and is thus aptly suited for this purpose. By projecting observed SSTs onto the SVD modes, it can be easily incorporated into an operational prediction scheme. The 6-month lag relationship between the SSR and large-scale SSTs provides a basis for developing long-range forecasting schemes for the occurrence of severe forest fire seasons in Canada. In so far as the global SSTs can be forecast with some accuracy, application of the statistical technique outlined in this paper can provide guidance to forest management officials.

[48] A number of statistical and dynamical procedures are already in place for the prediction of the ENSO-related SSTs. The usefulness of the statistical relationship outlined in this work will increase as predictions of SSTs extend into the global domain. This predictability may be further enhanced by the inclusion of direct measurements of winter snow cover as well as regional information related to soil and forest fuel moisture that are important to the development of severe forest fire conditions.

References

Barnett, T. P., and R. Preisendorfer (1987), Origins and levels of monthly and seasonal forecast skill for the United States surface air temperature determined by the canonical correlation analysis, *Mon. Weather Rev.*, *115*, 1825–1850.

Bonsal, B. R., and R. G. Lawford (1999), Teleconnections between El Nino and La Nina events and summer extended dry spells on the Canadian prairies, *Int. J. Climatol.*, *19*, 1445–1458.

Bonsal, B. R., A. K. Chakravarti, and R. G. Lawford (1993), Teleconnections between north Pacific SST anomalies and growing season extended dry spells on the Canadian Prairies, *Int. J. Climatol.*, *13*, 865–878.

Bretherton, C. S., C. Smith, and J. M. Wallace (1992), An intercomparison of methods for finding coupled patterns in climate data, *J. Clim.*, *5*, 541–560.

Cherry, S. (1997), Some comments on singular value decomposition analysis, *J. Clim.*, *10*, 1759–1761.

Czaja, A., and J. Marshall (2001), Observations of atmosphere ocean coupling in the North Atlantic, *Q. J. R. Meteorol. Soc.*, *127*, 1893–1916.

Deser, C., and M. L. Blackmon (1995), On the relationship between tropical and North Pacific sea surface temperature variations, *J. Clim.*, *8*, 1677–1680.

Ecological Stratification Working Group (1996), A national ecological framework for Canada, Agric. and Agri-Food Can., Ottawa, Ont., Canada.

Enfield, D. B., A. M. Mestas-Nuñez, and P. J. Trimble (2001), The Atlantic multidecadal oscillation and its relation to rainfall and river flows in the continental U.S., *Geophys. Res. Lett.*, *28*, 2077–2080.

Flannigan, M. D., and C. E. Van Wagner (1991), Climate change and wildfire in Canada, *Can. J. For. Res.*, *21*, 66–72.

Flannigan, M. D., and B. M. Wotton (1989), A study of interpolation methods for forest fire danger rating in Canada, *Can. J. For. Res.*, *19*, 1059–1066.

Flannigan, M. D., and B. M. Wotton (2001), Climate, weather and area burned, in *Forest Fires: Behavior and Ecological Effects*, edited by E. A. Johnson and K. Miyanishi, pp. 335–357, Elsevier, New York.

Flannigan, M. D., K. A. Logan, B. D. Amiro, W. R. Skinner, and B. J. Stocks (2005), Future area burned in Canada, *Clim. Change*, *21*, 66–72.

Folland, C. K., et al. (2001), Global temperature change and its uncertainties since 1861, *Geophys. Res. Lett.*, *28*, 2621–2624.

Gillett, N. P., A. J. Weaver, F. W. Zwiers, and M. D. Flannigan (2004), Detecting the effect of climate change on Canadian forest fires, *Geophys. Res. Lett.*, *31*, L18211, doi:10.1029/2004GL020876.

Harrington, J. B., M. D. Flannigan, and C. F. Van Wagner (1983), A study of the relation of components of the Fire Weather Index System to monthly provincial area burned by wildfire in Canada 1953–80, *Inf. Rep. PI-X-25*, Can. For. Serv., Petawawa Research Forest, Ont., Canada.

Hoerling, M., and A. Kumar (2003), The perfect ocean for drought, *Science*, *299*, 691–694.

Hurrell, J. W. (1996), Influences of variations in extratropical wintertime teleconnections on Northern Hemisphere temperature, *Geophys. Res. Lett.*, *23*, 665–668.

Iwasaka, N., and J. M. Wallace (1995), Large scale interaction in the Northern Hemisphere from a view point of variations of surface heat flux by SVD analysis, *J. Meteorol. Soc. Jpn.*, *73*, 781–794.

Lau, N.-C., and M. J. Nath (1994), A modeling study of the relative roles of tropical and extratropical anomalies in the variability of the global atmosphere-ocean system, *J. Clim.*, *7*, 1184–1207.

Levine, J. S. (Ed.) (1991), *Global Biomass Burning: Atmospheric, Climatic, and Biospheric Implications*, MIT Press, Cambridge, Mass.

Levine, J. S. (Ed.) (1996), *Biomass Burning and Global Change*, MIT Press, Cambridge, Mass.

Mantua, N. J., S. R. Hare, Y. Zhang, J. M. Wallace, and R. C. Francis (1997), A Pacific interdecadal climate oscillation with impacts on salmon production, *Bull. Am. Meteorol. Soc.*, *78*, 1069–1079.

Mestas-Nunez, A. M., and D. B. Enfield (1999), Rotated global modes of non-ENSO sea surface variability, *J. Clim.*, *12*, 2734–2746.

Newman, M., and P. D. Sardeshmukh (1995), A caveat concerning singular value decomposition, *J. Clim.*, *8*, 352–360.

Podur, J., D. L. Martell, and K. Knight (2002), Statistical quality control analysis of forest fire activity in Canada, *Can. J. For. Res.*, *32*, 195–205.

Reynolds, R. W., N. A. Rayner, T. M. Smith, D. C. Stokes, and W. Wang (2002), An improved in situ and satellite SST analysis, *J. Clim.*, *15*, 1609–1625.

Shabbar, A., and M. Khandekar (1996), The impact of El Niño–Southern Oscillation on the temperature field over Canada, *Atmos. Ocean*, *34*, 401–416.

Shabbar, A., and W. Skinner (2004), Summer drought patterns and the relationship to global sea surface temperatures, *J. Clim.*, *17*, 2866–2880.

Shabbar, A., B. Bonsal, and M. Khandekar (1997a), Canadian precipitation patterns associated with the Southern Oscillation, *J. Clim.*, *10*, 3016–3027.

Shabbar, A., K. Higuchi, W. Skinner, and J. L. Knox (1997b), The association between the BWA index and winter surface temperature variability over eastern Canada and west Greenland, *Int. J. Climatol.*, *17*, 1195–1210.

Skinner, W. R., B. J. Stocks, D. L. Martell, B. Bonsal, and A. Shabbar (1999), The association between circulation anomalies in the mid-troposphere and area burned by wildland fire in Canada, *Theor. Appl. Climatol.*, *63*, 89–105.

Skinner, W. R., J. B. Todd, M. D. Flannigan, D. L. Martell, B. J. Stocks, and B. M. Wotton (2002), A 500 mb synoptic wildland fire climatology from large Canadian forest fires, 1959–1996, *Theor. Appl. Climatol.*, *71*, 157–169.

Smith, T. M., and R. W. Reynolds (2003), Extended reconstruction of global sea surface temperatures based on COADS data (1854–1997), *J. Clim.*, *16*, 1495–1510.

Smith, T. M., R. W. Reynolds, R. E. Livezey, and D. Stokes (1996), Reconstruction of historical sea surface temperatures using empirical orthogonal functions, *J. Clim.*, *9*, 1403–1420.

Smith, T. M., R. E. Livezey, and S. S. Shen (1998), An improved method for analyzing sparse and irregularly distributed SST data on a regular grid: The tropical Pacific Ocean, *J. Clim.*, *11*, 1717–1729.

Stocks, B. J., B. S. Lee, and D. S. Martell (1996), Some potential carbon budget implications of fire management in the boreal forest, in *Forest Ecosystems, Forest Management and the Global Carbon Cycle*, *NATO ASI Ser., Ser. 1*, vol. 40, edited by M. J. Apps and D. T. Price, pp. 89–96, Springer, New York.

Stocks, B. J., et al. (2002), Large forest fires in Canada, 1959–1997, *J. Geophys. Res.*, *108*(D1), 8149, doi:10.1029/2001JD000484.

Van Wagner, C. E. (1970), Conversion of Williams Severity Rating for use with the Fire Weather Index, *Inf. Rep. PS-X-21*, Can. Dep. of Fish. and For., Petawawa For. Exp. Stn., Petawawa Research Forest, Ont., Canada.

Van Wagner, C. E. (1987), The development and structure of the Canadian Forest Fire weather index system, *For. Tech. Rep. 35*, Can. For. Serv., Ottawa, Ont., Canada.

von Storch, H., and F. W. Zwiers (1999), *Statistical Analysis in Climate Research*, 484 pp., Cambridge Univ. Press, New York.

Wallace, J. M., C. Smith, and C. S. Bretherton (1992), Singular value decomposition of wintertime sea surface temperature and 500-mb height anomalies, *J. Clim.*, *5*, 561–576.

Williams, D. E. (1959), Fire season severity rating, *Div. Tech. Note 73*, Can. Dep. of North. Affairs and Nat. Resour., Ottawa, Ont., Canada.

Woodruff, S. D., H. F. Diaz, J. D. Elms, and S. J. Worley (1998), COADS Release 2 data and metadata enhancements for improvements of marine surface flux fields, *Phys. Chem. Earth*, *23*, 517–527.

Zhang, Y., J. M. Wallace, and D. S. Batisti (1997), ENSO-like interdecadal variability: 1900–93, *J. Clim.*, *10*, 1004–1020.

————————

M. D. Flannigan and K. Logan, Great Lakes Forestry Centre, Canadian Forest Service, 1219 Queen Street East, Sault Ste. Marie, ON, Canada P6A 2E5.

A. Shabbar and W. R. Skinner, Climate Research Division, Environment Canada, 4905 Dufferin Street, Toronto, ON, Canada M3H 5T4. (walter.skinner@ec.gc.ca)